19.5% Efficiency in Binary Organic Solar Cells with Enhanced Stability Using a Flexible Chain-Tethered Dimeric Acceptor with Unprecedentedly High Yield

Qiqing Ruan,[a,†] Yue Ma,[a,†] Tianchen Pan,[b,†] Tianyi Zhang,[a] Yuan Su,[a] Lunbi Wu,[c] Yulong Hai,[b] Yao Li,[b] Yongmin Luo,[b] Qingduan Li,[a] Jifa Wu,[d] Ruijie Ma,[e,] Sha Liu,[f] Biao Xiao,[g] Tao Jia,[c] Xiaobin Peng,[d] Jiaying Wu,[b,*] Gang Li,[e,*] Yue-Peng Cai,[a] and Shengjian Liu [a,*]*

[a]School of Chemistry, Guangzhou Key Laboratory of Materials for Energy Conversion and Storage, Key Laboratory of Electronic Chemicals for Integrated Circuit Packaging, South China Normal University (SCNU), Guangzhou 510006, P. R. China

[b]Advanced Materials Thrust, Function Hub, The Hong Kong University of Science and Technology (Guangzhou), Nansha 511400, Guangzhou, P. R. China

[c]School of Optoelectronic Engineering, Guangdong Polytechnic Normal University, Guangzhou, 510665, P. R. China

[d]Institute of Polymer Optoelectronic Materials and Devices, State Key Laboratory of Luminescent Materials and Devices, South China University of Technology, Guangzhou 510640, P. R. China

[e]Department of Electrical and Electronic Engineering, Research Institute for Smart Energy (RISE), Photonic Research Institute (PRI), Guangdong-Hong Kong-Macao Joint Laboratory for Photonic-Thermal-Electrical Energy Materials and Devices, The Hong Kong Polytechnic University, Hong Kong, China

[f]Dongguan Key Laboratory of Interdisciplinary Science for Advanced Materials and Large-Scale Scientific Facilities, School of Physical Sciences, Great Bay University, Dongguan, Guangdong, 523000, P. R. China

[g]Key Laboratory of Optoelectronic Chemical Materials and Devices (Ministry of Education), Flexible Display Materials and Technology Co–Innovation Centre of Hubei Province, School of Optoelectronic Materials & Technology, Jianghan University, Wuhan 430056, P.R. China

[†]These authors contributed equally.

*Corresponding author

E-mail: ruijie.ma@polyu.edu.hk (Ruijie Ma); jiayingwu@ust.hk (Jiaying Wu); gang.w.li@polyu.edu.hk (Gang Li); shengjian.liu@m.scnu.edu.cn (Shengjian Liu);

Abstract

Herein, an alkyl-chain-linked strategy is employed to synthesize a dimeric acceptor, DPhC8Y, which achieves simultaneous enhancements in device efficiency and stability while also exhibiting an unprecedentedly high production yield compared to other "giant molecular acceptors" for organic solar cells (OSCs). Compared to the monomer DTY6, DPhC8Y contains improved crystalline ordering and refined phase separation, thereby reduced non-radiative loss, suppressed bulk and interface recombination, and decreased trap density. On the other hand, the dimer acceptor possesses intrinsically higher glass transition point. Through performance evaluation, binary device of D18:DPhC8Y blend demonstrates 19.50% efficiency with remarkably over 80% fill factor, surpassing those of D18:DTY6 (18.25% and 76.42%). Meanwhile, the dimer based active layer displays significantly enhanced storage and thermal stability in device. Our report showcases the possibility of achieving OSCs with concurrently decent efficiency, stability, and cost-effectiveness through smart material and synthesis design.

Keywords: Organic solar cells; Dimer acceptor; High synthesis yield; Device stability

Introduction

The emergence of "giant molecular acceptors" or oligomeric acceptors in recent years has opened new pathways in the field of organic solar cells (OSCs), enabling both high power conversion efficiencies (PCE > 19%) and exceptional device stability (T80 > 10,000 hours) simultaneously. [1-16] With ongoing advancements in material design and device engineering, devices based on oligomeric acceptors are expected to rival the state-of-the-art PCEs achieved by "monomer" acceptors.[17-27] Therefore, in the next stage, research on oligomeric acceptors should not only focus on efficiency but also address other critical metrics, such as synthesis complexity and overall yield, to advance their practical application. Currently, high-performance multimer acceptors are primarily synthesized using terminal group connection strategies, inspired by the design principles of polymer acceptors. [28-36] However, these molecules often require lengthy synthetic routes and exhibit relatively low yields due to the complex purification processes for non-isomerizable terminal groups and the low yields associated with synthesizing asymmetric intermediates. In contrast, the synthesis of oligomeric acceptors connected by alkyl chains avoids the aforementioned challenges and typically achieves a higher comprehensive yield; however, research on such acceptors remains less explored compared to those synthesized via terminal group connection strategies.

In this work, we report a dimeric acceptor, (2,2',2",2"'-((2Z,2'Z,2"Z,2"'Z)-(((((2,5-dibromo-1,4-phenylene)bis(oxy))bis(octane-8,1-diyl))bis(13-(2-decyltetradecyl)-3,9-diundecyl-12,13-dihydro-[1,2,5]thiadiazolo[3,4-e]thieno[2",3":4',5']thieno[2',3':4,5]pyrrolo[3,2-g]thieno[2',3':4,5]thieno[3,2-b]indole-12,2,10-triyl))tetrakis(methaneylylidene))tetrakis(5,6-difluoro-3-oxo-2,3-dihydro-1H-indene-2,1-diylidene))tetramalononitrile) (DPhC8Y), synthesized via an alkyl chain-linked strategy, with its monomer counterpart being the well-known small molecule acceptor (2,2'-((2Z,2'Z)-((12,13-bis(2-decyltetradecyl)-3,9-diundecyl-12,13-dihydro-[1,2,5]thiadiazolo[3,4-e]thieno[2",3":4',5']thieno[2',3':4,5]pyrrolo[3,2-g]thieno[2',3':4,5]thieno[3,2-b]indole-2,10-diyl)bis(methaneylylidene))bis(5,6-difluoro-3-oxo-2,3-dihydro-1H-indene-2,1-diylidene))dimalononitrile) (DTY6).[37]

The synthesis process comprises only four steps, each characterized by high yields, resulting in an overall yield as high as 56%. When fabricating bulk heterojunction (BHJ) OSCs, D18:DPhC8Y-based achieve a high PCE of 19.50% and a remarkable *FF* of 80.17%, significantly outperforming the control device based on D18:DTY6, which exhibits a PCE of 18.25%. Comprehensive characterizations reveal that the performance improvement is primarily attributed to an optimized charge generation process, reduced free-charge losses, and slightly suppressed non-radiative recombination, all resulting from refined phase distribution in the dimeric acceptor-based OSCs. Due to its higher molecular weight, the dimer molecule exhibits a greater glass transition temperature (T_g), effectively restricting molecular diffusion and enhancing thermal stability. As a result, DPhC8Y demonstrates superior thermal stability compared to DTY6, as evidenced by the 1200-hour tracking test. These findings provide new insights into molecular design strategies for improving the comprehensive performance of oligomeric acceptor-based OSCs, enabling simultaneous enhancements in efficiency, stability, and scalability.

Experimental Methods

3,9-Diundecyl-12,13-dihydro-[1,2,5]thiadiazolo[3,4-e]thieno[2'',3'':4',5']thieno[2',3':4,5]pyrrolo[3,2-g]thieno[2',3':4,5]thieno[3,2-b]indole (compound 1) were purchased from Solarmer. 2-(5,6-Difluoro-3-oxo-2,3-dihydro-1H-inden-1-ylidene)malononitrile was purchased from Bide Pharmatech Ltd. Other chemicals and solvents were obtained from commercial sources (Sigma Aldrich, Acros, Strem, or Alfa Aesar) and used as received. The experimental details are provided in the Supporting Information, including material synthesis, characterization, density functional calculations, OSCs fabrication and characterization, UV−Vis absorption, photoelectron spectroscopy in air (PESA), transient photocurrent (TPC) and transient photovoltage (TPV) measurements, energy loss, transient absorption spectroscopy and grazing incidence wide angle X-ray scattering (GIWAXS) measurements.

Results and Discussion

Molecular Design, Synthesis, and Basic Properties

The synthetic route of DPhC8Y is illustrated in **Scheme 1**. Inspired by a reported procedure, [38] **compound 1**, which is commercially available, is converted into the bromide alkyl-functionalized **compound 2** with a high yield of 81%. Subsequently, **compound 3** is obtained through a nucleophilic reaction between the 2,5-dibromobenzene-1,4-diol core and **compound 2**, achieving a yield of 81%. Next, a Vilsmeier-Haack reaction is employed to transform **compound 3** into **compound 4**, with an impressive yield of 94%. Finally, the target molecule **DPhC8Y** is synthesized from **compound 4** via a pyridine-catalyzed Knoevenagel condensation, yielding 90%. The overall synthesis yield of **DPhC8Y** reaches 56%, demonstrating its feasibility for large-scale production once commercial demand is established. The structural characterization results, including ^{1}H NMR, ^{13}C NMR, and mass spectra, are presented in **Figures S1** to **S9**. DPhC8Y exhibits excellent solubility in chloroform, ensuring its processability for solar cell fabrication in various scenarios. The intrinsic stability of DPhC8Y and DTY6 was evaluated using thermogravimetric analysis (TGA), as shown in **Figure S10**. Under a nitrogen atmosphere, the temperatures at which DPhC8Y and DTY6 lose 5% of their initial weight are 337 °C and 331 °C, respectively. These results indicate that both materials possess good thermal stability.

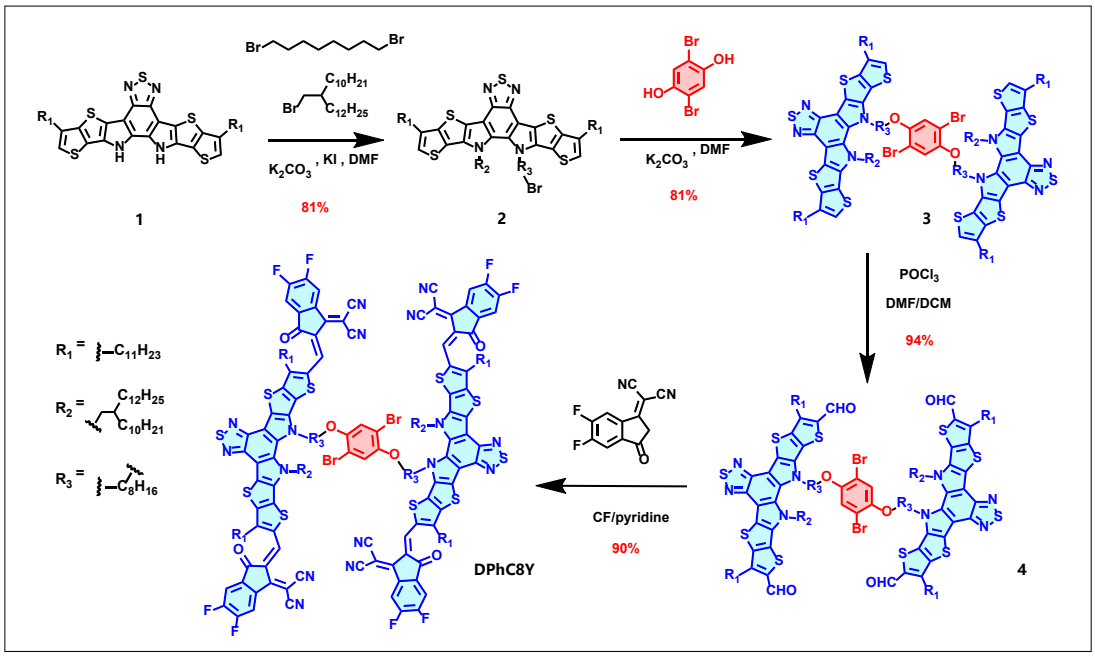

Scheme 1. The synthetic route of DPhC8Y marked with yield for each step.

For clarification, the chemical structures of D18, DTY6, and DPhC8Y are illustrated in **Figure 1a-c**. Their optical properties were investigated using ultraviolet-visible (UV-Vis) absorption measurements, with the normalized absorption spectra in solution and film states presented in **Figure 1d** and **1e**, respectively. D18 exhibits an enhanced shoulder peak relative intensity without a significant redshift, indicating strong pre-aggregation and good molecular packing in solution. Compared to DPhC8Y, DTY6 shows a blue-shifted absorption edge in diluted chloroform but a significantly redder photon response range in the film state. This suggests that the aggregation of the dimeric acceptor is more restricted, likely due to its larger molecular size. The crystallization characteristics of the two acceptors were further compared using differential scanning calorimetry (DSC), as shown in **Figure 1f.** The melting point (T_m) of DPhC8Y is 268 °C, significantly higher than that of DTY6 (192 °C), while the melting enthalpy (ΔH_m) of DPhC8Y is slightly reduced to 21.04 J/g compared to 22.16 J/g for DTY6. These findings indicate that good crystallinity can be retained while effectively restricting molecular motion. Next, the energetic structures of the three studied materials are evaluated using photoelectron spectroscopy in air (PESA) and inverse photoemission spectroscopy (IPES) measurements.[38, 39] As shown in **Figure S11** and **Figures 1g–h**, the energy level diagram of D18, DTY6, and DPhC8Y is illustrated in **Figure 1i**. The results indicate that DPhC8Y possesses a slightly lower electron affinity, which may contribute to achieving a higher open-circuit voltage (V_{OC}) in devices.

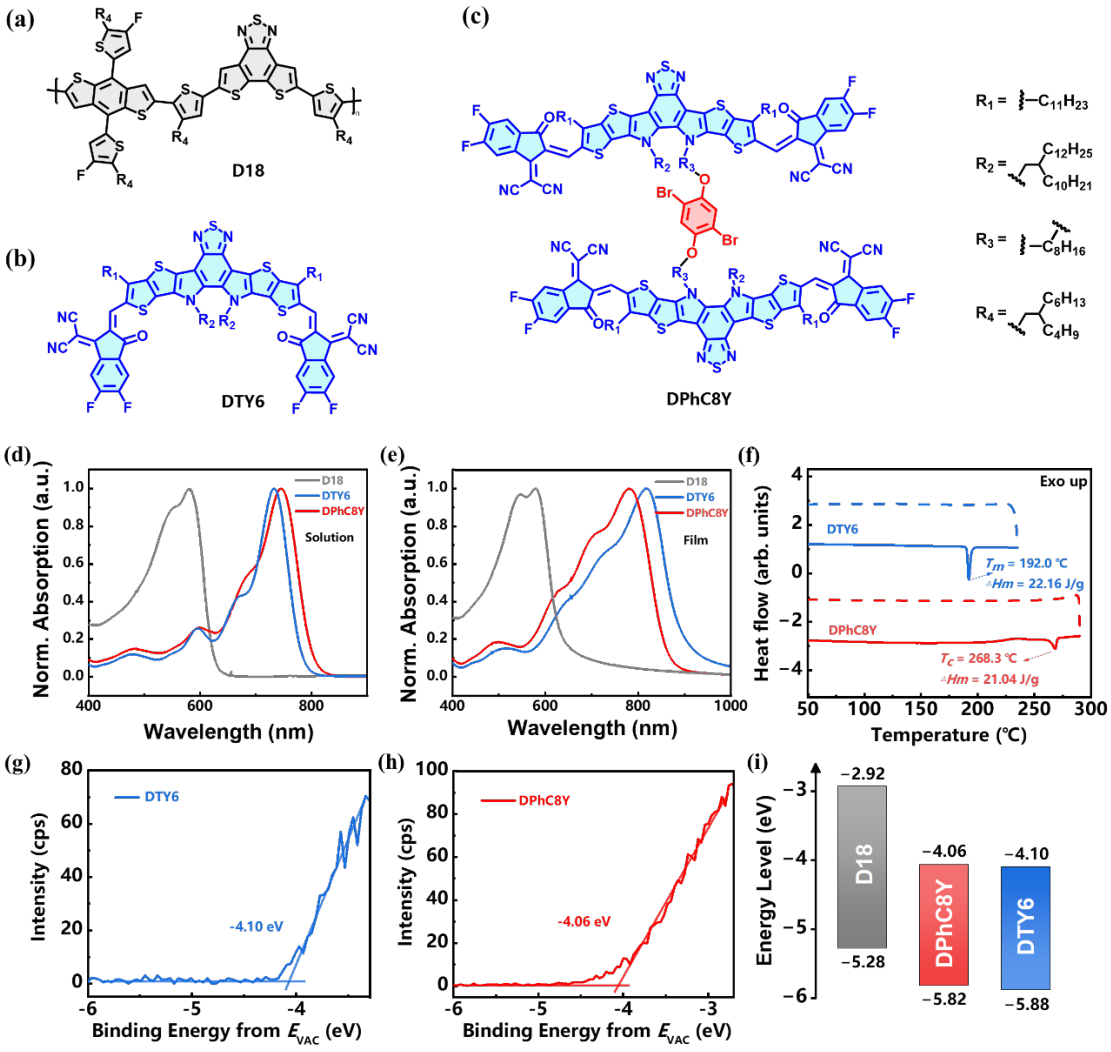

Figure 1. The chemical structures of (a) D18, (b) DTY6 and (c) DPhC8Y. The UV-vis spectra of D18, DTY6, and DPhC8Y (d) in solution and (e) in film state. (f) DSC curves of two acceptors. (g)(h) The IPES results for DTY6 and DPhC8Y. (i) The gained energy level diagram of D18, DTY6, and DPhC8Y.

Theoretical Calculations

In parallel, density functional theory (DFT) calculations are employed to compare the molecular packing and charge transport properties of DTY6 and DPhC8Y.[40, 41] Using the B3LYP/def2-SVP level of theory, the backbone geometries of D18, DTY6, and DPhC8Y were fully optimized. **Figure 2b** presents the electrostatic potential (ESP) distribution [42-44] mapped onto the molecular surfaces, where blue and red regions correspond to negative and positive ESP values, respectively. In both acceptor molecules, the negative ESP regions are primarily localized on nitrogen atoms, while the positive potentials are concentrated on the aromatic rings of the backbone.

Quantitative analysis reveals that DPhC8Y exhibits a superior charge balance parameter (ν = 0.221) compared to DTY6 (ν = 0.192), approaching the theoretical maximum of 0.250. This suggests an enhanced molecular interaction propensity in DPhC8Y. Furthermore, the average surface deviation values (6.68 kcal/mol for DPhC8Y versus 6.01 kcal/mol for DTY6) provide additional evidence of improved intramolecular charge separation in the designed acceptor. These combined results indicate that DPhC8Y possesses significantly greater molecular activation capability than DTY6, highlighting its potential for superior performance in organic photovoltaic devices.

To further investigate and compare the interactions between the acceptors and the donor, we analyze their intermolecular interactions. **Figure 2c** presents the Interaction Region Indicator (IRI) analysis [45-47] for D18:DTY6 and D18:DPhC8Y pairs, highlighting the nature and distribution of their non-covalent interactions. The color mapping identifies three distinct interaction regimes: strong attractive forces (blue regions), van der Waals interactions (green regions), and strong repulsive interactions (red regions). Notably, the D18:DPhC8Y system exhibits intensified weak interactions, as evidenced by the higher density of spikes in the green interaction zone. **Figure 2d** further illustrates the weak interaction regions in D18:DTY6 and D18:DPhC8Y, based on Independent Gradient Model-Hirshfeld (IGMH) analysis.[48, 49] The stronger van der Waals interactions observed in D18:DPhC8Y may be attributed to the interaction between D18 and the linker unit in DPhC8Y, which enhances molecular packing and potentially improves charge transport properties.

Based on MD simulations, we conducted a comparative analysis of molecular packing between the DPhC8Y and DTY6 systems using the framework shown in **Figure S13a** Calculated minimum intermolecular distances (DTY6: 0.203 nm, DPhC8Y: 0.201 nm, see **Figure S13b**) reveal that the slightly smaller spacing in DPhC8Y may enhance interactions with donor materials like D18, likely attributable to alkyl chain-induced morphological modifications that optimize interfacial contact and potentially improve *FF*. Free volume analysis (**Figure S13c**) further suggests comparable or marginally tighter packing in DPhC8Y relative to DTY6 (<1% difference). Given these minimal variations in both intermolecular distances and free

volumes, we conclude that the overall molecular packing arrangement remains similar between the two systems despite localized structural adjustments from linker design.

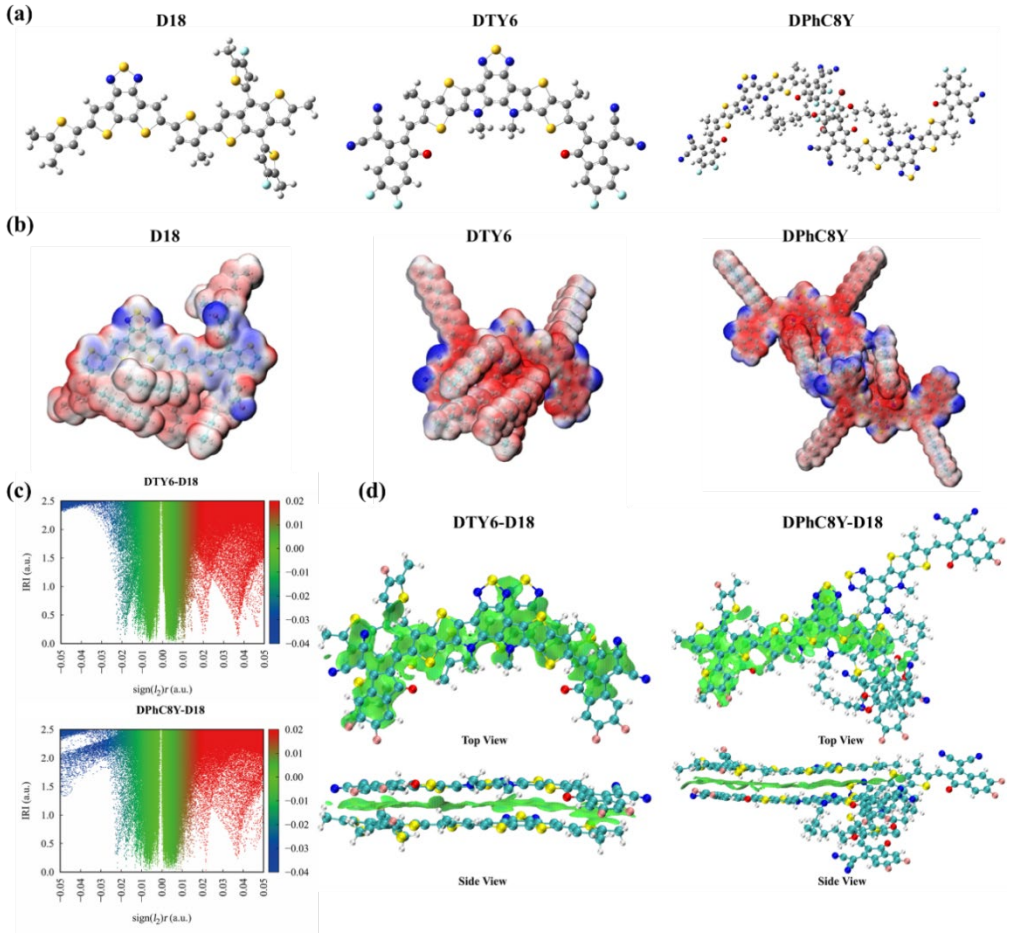

Figure 2. (a) Optimized molecular backbone structures and (b) electrostatic potential (ESP) surface maps of D18, DTY6 and DPhC8Y. (c) correlation between Interaction Region Indicator (IRI) and Sign(λ_2)ρ profiles for D18:DTY6 and D18:DPhC8Y. (d) Hirshfeld-partitioned Independent Gradient Model (IGMH) visualizations showing top and side views of Van der Waals interaction regions.

Photovoltaic Performance, Charge Generation, Transport, and Recombination

Then, the photovoltaic performances of DTY6 and DPhC8Y are studied by a series of devices with conventional structure ITO/ Poly(3,4-ethylenedioxythiophene)-poly(styrenesulfonate) (PEDOT:PSS)/ (2-(9H-carbazol-9-yl)ethyl)phosphonic acid (2PACz)/ active layer/ (poly[[2,7-bis(2-ethylhexyl)-1,2,3,6,7,8-hexahydro-1,3,6,8-tetraoxobenzo[lmn][3,8]phenanthroline-4,9-diyl]-2,5-thiophenediyl[9,9-bis[3-(dimethylamino)propyl]-9H-fluorene-2,7-diyl]-2,5-thiophenediyl) (PNDIT-F_3N)/ Ag.[50, 51] The current density versus voltage (*J-V*) characteristics of them are plotted in

Figure 3a, and corresponding parameters are extracted as shown by **Table 1**. As observed, D18:DPhC8Y-based devices achieve an impressive PCE of 19.50%, primarily driven by an improved *FF* and partially attributed to an increase in open-circuit voltage (V_{OC}). Notably, this high PCE ranks among the state-of-the-art efficiencies for oligomeric acceptor OSCs. To compare the photon harvesting differences between DTY6 and DPhC8Y in the active layer, the external quantum efficiency (EQE) spectra of the optimal devices were measured and are presented in **Figure 3b**. The photon response edges of both systems are nearly identical, suggesting that blending with D18 induces different degrees of spectral blueshift in the two acceptors. Although the maximum response of the D18:DTY6-based device reaches 92%, its calculated current density (J_{cal}) is not higher than that of the D18:DPhC8Y blend due to less efficient photon absorption in the 550–650 nm range. Additionally, the similar spectral tails indicate that the D18:DPhC8Y-based device exhibits more suppressed voltage loss. To further emphasize the significance of this work, **Table S1** and **Figure 3c** provide a summary of recent reports on oligomeric acceptors, including DPhC8Y, in terms of PCE and synthesis yields. This comparison further substantiates our claim of achieving both high device efficiency and cost-effective synthesis. The charge generation, transport, and recombination behaviors of the corresponding devices were further investigated. As shown in Figure S14, the photocurrent density (J_{ph}) increases rapidly with rising effective voltage (V_{eff}) at low voltage regions and gradually reaches a saturation value (J_{sat}) before V_{eff} approaches 2.0 V. Based on the ratio of J_{SC} to J_{sat}, the exciton dissociation efficiencies (P_{diss}) of the D18:DTY6 and D18:DPhC8Y-based OSCs were calculated to be 98.1% and 99.1%, respectively. Furthermore, the charge collection efficiencies (P_{coll}), determined from the ratio of $J_{ph,max}$ (J_{ph} at the maximum power output point) to J_{sat}, were 88.9% and 89.3%, respectively. Following this investigation, the charge transport properties were evaluated for both active systems by fabricating hole-only and electron-only devices and analyzing them using the space charge limited current (SCLC) method. The $J^{1/2}$-V curves of these devices are presented in **Figure S15**, with the calculated hole and electron mobilities summarized

in **Table S2** and **Figure 3d**. For the D18:DTY6 and D18:DPhC8Y-based devices, the hole and electron mobilities were determined to be $1.22\times10^{-3}/1.06\times10^{-3}$ and 1.39×10^{-3} $/1.32\times10^{-3}$ $cm^2\cdot V^{-1}\cdot s^{-1}$, respectively. These results further validate the improved charge transport characteristics of the D18:DPhC8Y-based system. Furthermore, charge recombination and extraction processes were analyzed through transient photocurrent (TPC) and transient photovoltage (TPV) measurements.[52, 53] As shown in **Figures 3e** and **3f**, the charge extraction time for the D18:DPhC8Y-based solar cell is 0.49 μs, slightly shorter than that of the D18:DTY6-based device (0.52 μs), which aligns with the conclusion drawn from the J_{ph} vs V_{eff} relationship.

Meanwhile, the recombination lifetime exhibits a more significant increase from 24 μs in the D18:DTY6-based device to 33 μs in the D18:DPhC8Y-based device, supporting the observed enhancement in *FF* from 76.4% to 80.2%. Additionally, the trap density of states (t-DOS) of both systems were investigated using capacitance-frequency spectroscopy (**Figure 3g**).[54, 55] The D18:DPhC8Y-based device exhibits lower trap state energy levels (0.514 eV) and trap density (2.14×10^{15} cm^{-3}) compared to the D18:DTY6 film (0.523 eV, 2.68×10^{15} cm^{-3}). Moreover, the voltage loss minimization in the D18:DPhC8Y system is further confirmed through a systematic analysis based on electroluminescence EQE (EQE-EL) and Fourier-transform photocurrent spectroscopy EQE (FTPS-EQE) measurements.[56] The FTPS-EQE and EQE-EL results are shown in **Figure S16**, while key parameters, including energy loss (E_{loss}), bandgap (E_g), black radiation loss (ΔE_1), radiative loss below the bandgap (ΔE_2), and non-radiative loss (ΔE_3) are listed in **Table S3** and visualized in **Figure 3h**. The D18:DPhC8Y-based device exhibits a larger E_g of 1.442 eV compared to 1.425 eV for the D18:DTY6 system, corresponding to E_{loss} values of 0.538 eV and 0.544 eV, respectively, indicating the dimeric DPhC8Y can result in a slight E_{loss} primarily due to a minimized ΔE_3, supported by an enhanced EQE-EL of 2.50×10^{-4}. The stability of the two active systems was evaluated by monitoring device performance under storage conditions. As shown in **Figure 3i**, D18:DPhC8Y-based devices retained over 87% of their initial PCE after 1200 hours of thermal annealing at 50 °C, outperforming D18:DTY6-based devices, which maintained 82% of their original efficiency.

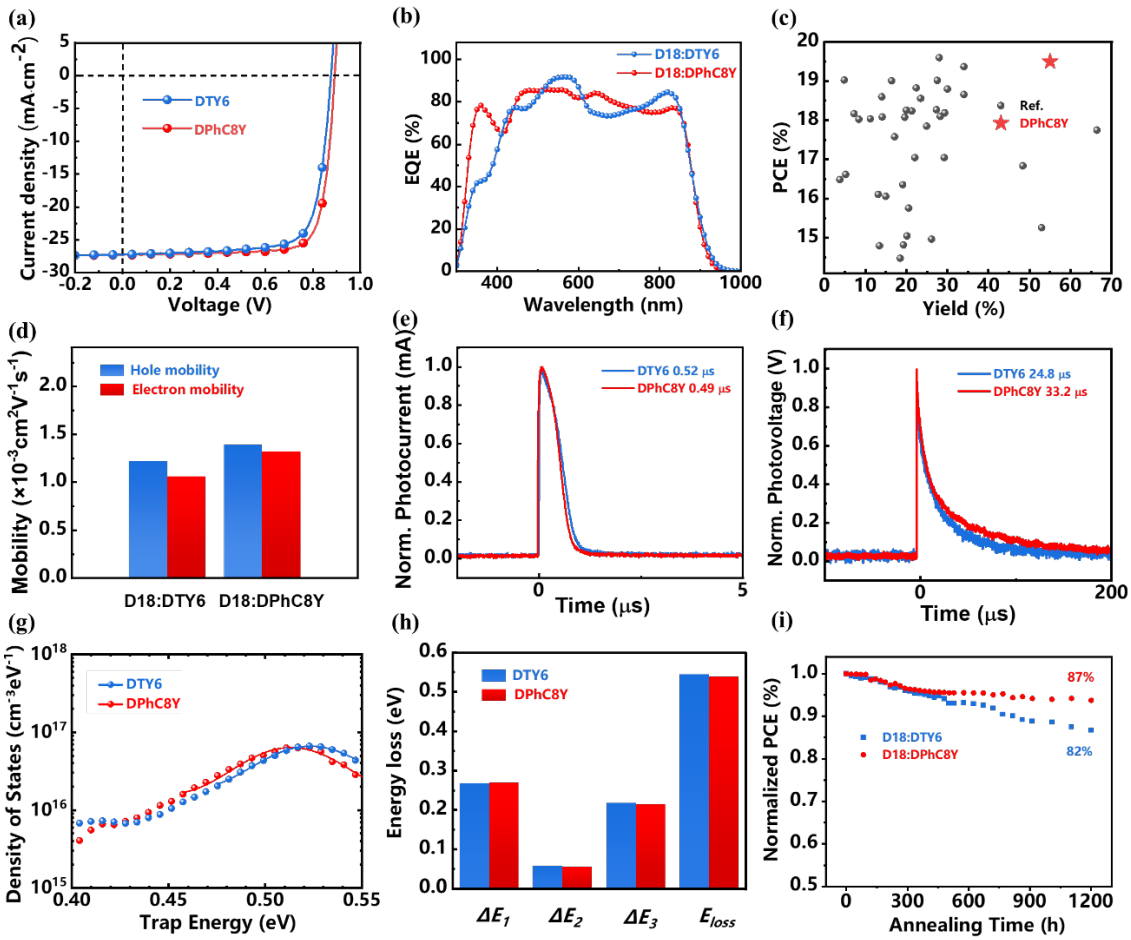

Figure 3. (a) *J-V* characteristics. (b) EQE spectra. (c) Performance comparison of this work and previous reports. (d) Hole and electron mobility. (e) The normalized TPC curves. (f) The normalized TPV curves. (g) The t-DOS curves. (h) The energy loss parameter summary. (i) The degradation of the related devices during heating at 50 °C, obtained from the average of five devices.

Table 1. Photovoltaic parameters of OSCs.

D18:acceptor	V_{OC} (V)	J_{SC}/J_{cal} (mA/cm^{-2})	*FF* (%)	PCE (%)
DTY6	0.88	27.24/25.99	76.4	18.25
DPhC8Y	0.89	27.28/26.31	80.2	19.50

Charge Generation and Recombination Kinetics

The charge generation and recombination processes are further examined using femtosecond transient absorption spectroscopy (fs-TAS).[57-59] The 2D contour maps and representative time spectral lines of neat acceptor and blend films are shown in **Figures 4a** to **4h**. The ground state bleaching (GSB) signal at approximately 580 nm is selected to track polaron kinetics, representing charge generation and recombination

dynamics at the donor/acceptor interface, where exciton dissociation occurs. As illustrated in **Figure 4i**, the dimeric acceptor-based active layer exhibits a faster charge generation rate and a prolonged recombination period, indicating more efficient hole transfer and suppressed non-geminate recombination. This finding further supports the enhanced EQE response in the 550–650 nm range observed for the D18:DPhC8Y-based device.

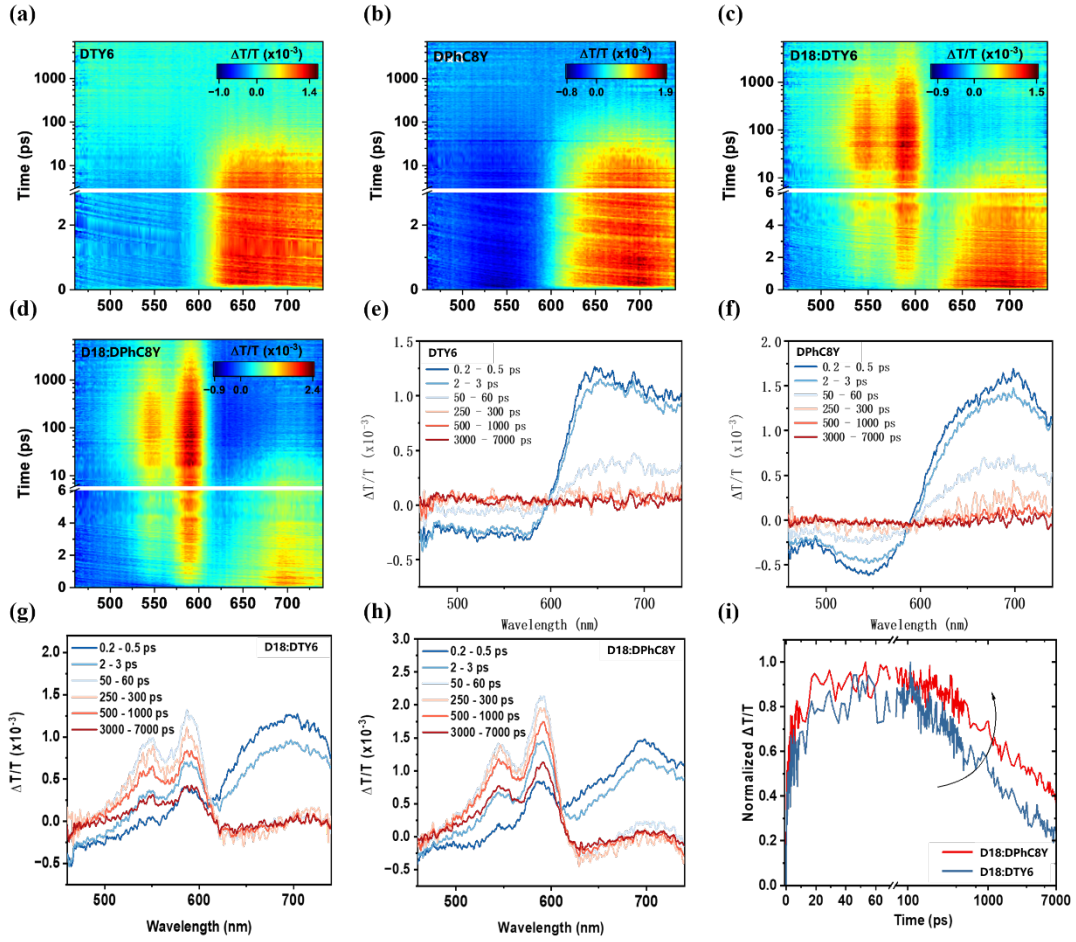

Figure 4. 2D contour maps of fs-TAS results for (a) DTY6, (b) DPhC8Y, (c) D18:DTY6, and (d) D18:DPhC8Y. Related spectral lines for (e) DTY6, (f) DPhC8Y, (g) D18:DTY6, and (h) D18:DPhC8Y. (i) The extracted polaron kinetics.

Morphology and Molecular Packing Characterizations

Following a detailed discussion on device physics and charge behavior, the focus shifts to the active layer morphology. The morphology is first examined using atomic force microscopy (AFM) and photo-induced force microscopy (PiFM).[60, 61] The corresponding images are presented in Figures 5a and 5b. Compared to the D18:DTY6 control film, the D18:DPhC8Y blend exhibits a significantly more refined fibrillar

structure while maintaining continuous donor and acceptor pure phases. This may indicate that the optimized dimerization approach enhances the charge generation and transport pathways without compromising phase continuity, further improving device performance. The phase separation optimization of DPhC8Y within the D18 polymer matrix is analyzed from both thermodynamic and crystallization kinetics perspectives.[62, 63] To assess this, contact angle measurements using water and diiodomethane (DIM) were conducted on neat donor and acceptor films (**Figure S17**). Based on a widely adopted calculation model, surface free energy and interaction parameters were determined, as summarized in **Table S4**.[64, 65] The results indicate that D18 and DPhC8Y exhibit better miscibility than D18 and DTY6, with interaction parameters of 0.54 K versus 0.88 K. Enhanced donor-acceptor miscibility is advantageous for forming a refined interpenetrating network in the blend film, contributing to improved device performance from a thermodynamic perspective. Meanwhile, the crystalline properties of these materials were systematically examined using grazing incidence wide-angle X-ray scattering (GIWAXS).[66, 67] The 2D diffraction patterns are displayed in **Figure 5c** and **Figure S18**, with corresponding line-cut profiles presented in **Figure 5d**. Compared to DPhC8Y, DTY6 exhibits multiple diffraction peaks, indicating a stronger aggregation tendency and higher crystallinity. However, the dimeric acceptor DPhC8Y demonstrates a more ordered packing motif despite its reduced crystallization tendency. As shown in **Tables S5–S8**, the out-of-plane (010) peak of the DPhC8Y neat film is located at 1.76 $Å^{-1}$, slightly higher than DTY6(1.75 $Å^{-1}$), further suggesting enhanced molecular ordering. When blended with D18, the π-π stacking peak of the D18:DPhC8Y film shifts to 1.73 $Å^{-1}$, compared to 1.72 $Å^{-1}$ for the D18:DTY6 blend, signifying inherently tighter molecular packing. Additionally, the crystalline coherence length (CL) of this peak is 13.6 Å for D18:DPhC8Y, versus 12.7 Å for D18:DTY6, confirming more ordered π-π stacking, which is advantageous for charge transport, aligning with the mobility test results discussed earlier. Furthermore, the diffraction intensity of the D18:DPhC8Y blend is significantly weaker than that of D18:DTY6, indicating the controllable aggregation

and crystallization tendency of the dimeric acceptor. This observation supports the notion that donor-acceptor phase separation is mitigated, leading to the formation of thinner nanofibers, as previously observed.

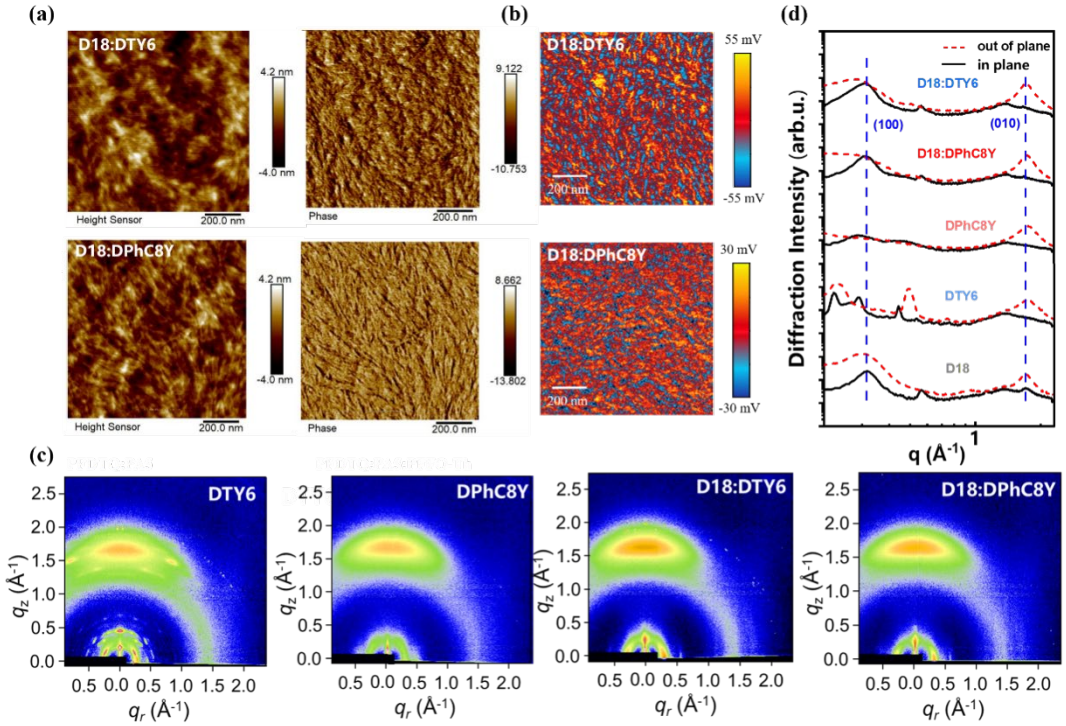

Figure 5. (a) AFM height and phase images and (b) PiFM images of two active layers. (c) 2D GIWAXS patterns. (d) IP and OOP line-cuts.

Conclusion

In this work, we successfully achieved a high PCE in oligomeric acceptor-based OSCs while keeping the synthesis yield at a decently high level. After alkyl chain connection, the dimeric molecule DPhC8Y exhibits appropriately reduced crystallinity compared to its monomer counterpart DTY6, enabling a more refined interpenetrating fibrillar network that optimizes donor-acceptor phase separation in the active layer. Consequently, the target device exhibits enhanced charge generation, reduced recombination, accelerated charge transport, and minimized non-radiative loss. Thanks to these improvements, the binary OSC based on D18:DPhC8Y achieves an impressive efficiency of 19.50%, ranking among the highest reported to date. Furthermore, the stability of the dimerized acceptor system is reaffirmed through systematic

investigations. This work not only delivers outstanding comprehensive device performance but also provides new chemical insights that could guide future advancements toward the commercialization of this research field.

Supporting Information

Supporting Information is available and includes additional details on general methods, experimental section, supporting Figures (Figures S1–S18) and supporting Tables S1–S10.

Conflict of Interest

The authors declare no competing financial interest.

Author Contribution

Qiqing Ruan: Investigation, Formal Analysis, Writing-Original Draft

Yue Ma: Investigation, Formal Analysis

Tianchen Pan: Formal Analysis, Methodology, Writing-Original Draft

Tianyi Zhang: Investigation, Formal Analysis

Yuan Su: Investigation, Formal Analysis

Lunbi Wu: Investigation, Formal Analysis

Yulong Hai: Formal Analysis, Methodology, Writing-Original Draf

Yao Li: Formal Analysis, Methodology, Writing-Original Draf

Yongmin Luo: Formal Analysis, Methodology

Qingduan Li: Investigation, Formal Analysis

Jifa Wu: Resources

Ruijie Ma: Conceptualization, Project Administration, Supervision, Writing-Original Draft

Sha Liu: Resources

Biao Xiao: Resources

Tao Jia: Investigation, Formal Analysis, Writing-Original Draft

Xiaobin Peng: Resources

Jiaying Wu: Resources, Funding Acquisition, Supervision

Gang Li: Resources, Funding Acquisition, Supervision

Yue-Peng Cai: Resources, Funding Acquisition, Supervision

Shengjian Liu: Conceptualization, Project Administration, Supervision, Writing-Original Draft

Acknowledgments

Shengjian Liu acknowledges the financial support from Natural Science Foundation of China (No. 21805097), the Guangdong Natural Science Foundation (No. 2021B1515120073), and the Guangdong Provincial Science and Technology Foundation (No. 2022A0505050068). Gang Li acknowledges Research Grants Council of Hong Kong (C4005-22Y, RGC Senior Research Fellowship Scheme (SRFS2223-5S01). Ruijie Ma acknowledges the support from PolyU Distinguished Postdoctoral Fellowship (1-YW4C). Jiaying Wu acknowledges the funding support from the National Natural Science Foundation of China (52303249), the Department of Science and Technology of Guangdong Province (2021QN02C110), the Guangzhou Municipal Science and Technology Bureau Projects (No. 2023A03J0097, No. 2023A03J0003, 2024A04J4513). Jiayig Wu also acknowledge the Green *e* Materials Laboratory for their facilities and technical support.

References

[1] J.-W. Lee, J. S. Park, H. Jeon, S. Lee, D. Jeong, C. Lee, Y.-H. Kim, B. J. Kim, *Chem. Soc. Rev.* **2024**, *53*, 4674-4706.

[2] J.-W. Lee, C. Sun, J. Lee, D. J. Kim, W. J. Kang, S. Lee, D. Kim, J. Park, T. N.-L. Phan, Z. Tan, F. S. Kim, J.-Y. Lee, X. Bao, T.-S. Kim, Y.-H. Kim, B. J. Kim, *Adv. Energy Mater.* **2024**, *14*, 2303872.

[3] M. Lv, Q. Wang, J. Zhang, Y. Wang, Z.-G. Zhang, T. Wang, H. Zhang, K. Lu, Z. Wei, D. Deng, *Adv. Mater.* **2024**, *36*, 2310046.

[4] B. Chang, Y. Zhang, C. Zhang, M. Zhang, Q. Wang, Z. a. Xu, Q. Chen, Y. Bai, H. Fu, S. Meng, L. Xue, S. Kim, C. Yang, Y. Yi, Z.-G. Zhang, *Angew. Chem. Int. Ed.* **2024**, *63*, e202400590.

[5] Y. Liang, D. Zhang, Z. Wu, T. Jia, L. Lüer, H. Tang, L. Hong, J. Zhang, K. Zhang, C. J. Brabec, N. Li, F. Huang, *Nat. Energy* **2022**, *7*, 1180-1190.

[6] C. Wang, X. Ma, Y.-f. Shen, D. Deng, H. Zhang, T. Wang, J. Zhang, J. Li, R. Wang, L. Zhang, Q. Cheng, Z. Zhang, H. Zhou, C. Tian, Z. Wei, *Joule* **2023**, *7*, 2386-2401.

[7] R. Zeng, J. Deng, X. Xue, S. Tan, L. Kan, Y. Lin, W. Zhong, L. Zhu, F. Han, Y. Zhou, X. Gao, M. Zhang, Y. Zhang, S. Xu, F. Liu, *Angew. Chem. Int. Ed.* **2025**, *64*, e202420453.

[8] Z. Zhang, S. Yuan, T. Chen, J. Wang, Y.-Q.-Q. Yi, B. Zhao, M. Li, Z. Yao, C. Li, X. Wan, G. Long, B. Kan, Y. Chen, *Energy Environ. Sci.* **2024**, *17*, 5719-5729.

[9] M. Ou, S. Xiong, X. Shen, H. Lai, X. Lai, Y. Wang, H. Li, F. He, *Macromolecules* **2024**, *57*, 4167-4173.

[10] C. Sun, J. Wang, F. Bi, H. Jiang, C. Yang, Y. Li, J. Chu, X. Bao, *Energy Environ. Sci.* **2025**, *18*, 862-873.

[11] H. Zhuo, X. Li, J. Zhang, S. Qin, J. Guo, R. Zhou, X. Jiang, X. Wu, Z. Chen, J. Li, L. Meng, Y. Li, *Angew. Chem. Int. Ed.* **2023**, *62*, e202303551.

[12] K. Yang, M. Lv, Y. Chang, K. Lu, Z. Wei, *Chinese Chem. Lett.* **2024**, *35*, 109018.

[13] C. Wang, X. Ma, D. Deng, H. Zhang, R. Sun, J. Zhang, L. Zhang, M. Wu, J. Min, Z.-G. Zhang, Z. Wei, *Nat. Commun.* **2024**, *15*, 8494.

[14] Y. Li, L. Mei, Z. Ge, C. Liu, J. Song, Y. Man, J. Gao, J. Zhang, Z. Tang, X.-K. Chen, Y. Sun, *Adv. Mater.* **2024**, *36*, 2403890.

[15] T. Jia, T. Lin, Y. Yang, L. Wu, H. Cai, Z. Zhang, K. Lin, Y. Hai, Y. Luo, R. Ma, Y. Li, T. A. Dela Peña, S. Liu, J. Zhang, C. Liu, J. Chen, J. Wu, S. Liu, F. Huang, *Nat. Commun.* **2025**, *16*, 871.

[16] J. Wang, C. Sun, Y. Li, F. Bi, H. Jiang, C. Yang, X. Bao, J. Chu, *Nat. Commun.* **2025**, *16*, 1784.

[17] W. A. Memon, Z. Deng, F. He, *EnergyChem* **2024**, *6*, 100129.

[18] Q. Bei, B. Zhang, K. Wang, S. Zhang, G. Xing, C. Cabanetos, *Chinese Chem. Lett.* **2024**, *35*, 108438.

[19] Y. Jiang, S. Sun, R. Xu, F. Liu, X. Miao, G. Ran, K. Liu, Y. Yi, W. Zhang, X. Zhu, *Nat. Energy* **2024**, *9*, 975-986.

[20] Z. Luo, W. Wei, R. Ma, G. Ran, M. H. Jee, Z. Chen, Y. Li, W. Zhang, H. Y. Woo, C. Yang, *Adv. Mater.* **2024**, *36*, 2407517.

[21] X. Gu, Y. Wei, R. Zeng, J. Lv, Y. Hou, N. Yu, S. Tan, Z. Wang, C. Li, Z. Tang, Q. Peng, F. Liu, Y. Cai, X. Zhang, H. Huang, *Angew. Chem. Int. Ed.* **2025**, *64*, e202418926.

[22] S. Guan, Y. Li, C. Xu, N. Yin, C. Xu, C. Wang, M. Wang, Y. Xu, Q. Chen, D. Wang, L. Zuo, H. Chen, *Adv. Mater.* **2024**, *36*, 2400342.

[23] L. Zhu, M. Zhang, G. Zhou, Z. Wang, W. Zhong, J. Zhuang, Z. Zhou, X. Gao, L. Kan, B. Hao, F. Han, R. Zeng, X. Xue, S. Xu, H. Jing, B. Xiao, H. Zhu, Y. Zhang, F. Liu, *Joule* **2024**, *8*, 3153-3168.

[24] N. Wei, J. Chen, Y. Cheng, Z. Bian, W. Liu, H. Song, Y. Guo, W. Zhang, Y. Liu, H. Lu, J. Zhou, Z. Bo, *Adv. Mater.* **2024**, *36*, 2408934.

[25] J. Song, C. Zhang, C. Li, J. Qiao, J. Yu, J. Gao, X. Wang, X. Hao, Z. Tang, G. Lu, R. Yang, H. Yan, Y. Sun, *Angew. Chem. Int. Ed.* **2024**, *63*, e202404297.

[26] J. Wang, P. Wang, T. Chen, W. Zhao, J. Wang, B. Lan, W. Feng, H. Liu, Y. Liu, X. Wan, G. Long, B. Kan, Y. Chen, *Angew. Chem. Int. Ed.* **2025**.

[27] J. Wang, Z. Zheng, P. Bi, Z. Chen, Y. Wang, X. Liu, S. Zhang, X. Hao, M. Zhang, Y. Li, J. Hou, *Natl. Sci. Rev.* **2023**, *10*, nwad085.

[28] Z. Luo, T. Liu, R. Ma, Y. Xiao, L. Zhan, G. Zhang, H. Sun, F. Ni, G. Chai, J. Wang, C. Zhong, Y. Zou, X. Guo, X. Lu, H. Chen, H. Yan, C. Yang, *Adv. Mater.* **2020**, *32*, 2005942.

[29] H. Sun, B. Liu, Y. Ma, J.-W. Lee, J. Yang, J. Wang, Y. Li, B. Li, K. Feng, Y. Shi, B. Zhang, D. Han, H. Meng, L. Niu, B. J. Kim, Q. Zheng, X. Guo, *Adv. Mater.* **2021**, *33*, 2102635.

[30] R. Sun, T. Wang, Q. Fan, M. Wu, X. Yang, X. Wu, Y. Yu, X. Xia, F. Cui, J. Wan, X. Lu, X. Hao, A. K. Y. Jen, E. Spiecker, J. Min, *Joule* **2023**, *7*, 221-237.

[31] R. Ma, H. Li, T. A. Dela Peña, X. Xie, P. W.-K. Fong, Q. Wei, C. Yan, J. Wu, P. Cheng, M. Li, G. Li, *Adv. Mater.* **2024**, *36*, 2304632.

[32] J. Song, C. Li, H. Ma, B. Han, Q. Wang, X. Wang, D. Wei, L. Bu, R. Yang, H. Yan, Y. Sun, *Adv. Mater.* **2024**, *36*, 2406922.

[33] J. Wang, Y. Li, C. Han, L. Chen, F. Bi, Z. Hu, C. Yang, X. Bao, J. Chu, *Energy Environ. Sci.* **2024**, *17*, 4216-4227.

[34] J. Wang, C. Han, S. Wen, F. Bi, Z. Hu, Y. Li, C. Yang, X. Bao, J. Chu, *Energy Environ. Sci.* **2023**, *16*, 2327-2337.

[35] Z. Wang, X. Wang, L. Tu, H. Wang, M. Du, T. Dai, Q. Guo, Y. Shi, E. Zhou, *Angew. Chem. Int. Ed.* **2024**, *63*, e202319755.

[36] Z. Wang, Y. Guo, X. Liu, W. Shu, G. Han, K. Ding, S. Mukherjee, N. Zhang, H.-L. Yip, Y. Yi, H. Ade, P. C. Y. Chow, *Nat. Commun.* **2024**, *15*, 1212.

[37] S. Dong, T. Jia, K. Zhang, J. Jing, F. Huang, *Joule* **2020**, *4*, 2004-2016.

[38] W. T. Hadmojo, F. H. Isikgor, Y. Lin, Z. Ling, Q. He, H. Faber, E. Yengel, R. Ali, A. Samad, R. E. A. Ardhi, S. Y. Jeong, H. Y. Woo, U. Schwingenschlögl, M. Heeney, T. D. Anthopoulos, *Energy Environ. Mater.* **2024**, *7*, e12712.

[39] J. Bertrandie, J. Han, C. S. P. De Castro, E. Yengel, J. Gorenflot, T. Anthopoulos, F. Laquai, A. Sharma, D. Baran, *Adv. Mater.* **2022**, *34*, 2202575.

[40] T. Lin, Y. Hai, Y. Luo, L. Feng, T. Jia, J. Wu, R. Ma, T. A. Dela Peña, Y. Li, Z. Xing, M. Li, M. Wang, B. Xiao, K. S. Wong, S. Liu, G. Li, *Adv. Mater.* **2024**, *36*, 2312311.

[41] T. Wang, J.-L. Brédas, *J. Am. Chem. Soc.* **2021**, *143*, 1822-1835.

[42] J. S. Murray, T. Brinck, P. Lane, K. Paulsen, P. Politzer, *J. Mol. Struct.: THEOCHEM* **1994**, *307*, 55-64.

[43] P. V. Bijina, C. H. Suresh, S. R. Gadre, *J. Comput. Chem.* **2018**, *39*, 488-499.

[44] P. K. Anjalikrishna, C. H. Suresh, S. R. Gadre, *J. Phys. Chem. A* **2019**, *123*, 10139-10151.

[45] N. Gillet, R. Chaudret, J. Contreras-García, W. Yang, B. Silvi, J.-P. Piquemal, *J. Chem. Theory Comput.* **2012**, *8*, 3993-3997.

[46] P. de Silva, C. Corminboeuf, *J. Chem. Theory Comput.* **2014**, *10*, 3745-3756.

[47] T. Lu, Q. Chen, *Chem. Methods* **2021**, *1*, 231-239.

[48] T. Lu, Q. Chen, *J. Comput. Chem.* **2022**, *43*, 539-555.

[49] T. Lu, Q. Chen, in *Compr. Comput. Chem.* (Eds.: M. Yáñez, R. J. Boyd), Elsevier, Oxford, **2024**, pp. 240-264.

[50] Z. Ge, J. Qiao, J. Song, X. Li, J. Fu, Z. Fu, J. Gao, X. Tang, L. Jiang, Z. Tang, G. Lu, X. Hao, Y. Sun, *Adv. Energy Mater.* **2024**, *14*, 2400203.

[51] S. Liu, L. Hao, J. Yu, Y. Xu, Y. Dou, J. Xie, Y. Wang, K. Zhang, F. Huang, Y. Cao, *ACS Nano* **2025**, *19*, 748-759.

[52] W. Su, X. Zhou, Z.-F. Yao, H. Bai, Y. Duan, R. Sun, Y. Wu, Q. Wu, H. Qin, C. Zhao, W. Zhu, H. Y. Woo, J. Min, Y. Li, W. Ma, Q. Fan, *Adv. Funct. Mater.* **2024**, *34*, 2313744.

[53] Y. Wang, Q. Chen, S. Liang, D. Xia, C. Zhao, C. R. McNeill, W. Li, *Chin. Chem. Lett.* **2024**, *35*, 109164.

[54] X. Qiao, R. Zhu, D. Yan, Z. Su, Z. Zhang, H. Wu, Y. Tan, M. Liang, W. Zuo, J. Zhang, G. Li, X. Gao, M. Saliba, M. Li, *Adv. Funct. Mater.* **2024**, *34*, 2409852.

[55] S. Leng, T. Hao, G. Zhou, L. Zhu, W. Zhong, Y. Yang, M. Zhang, J. Xu, J. Zhan, Z. Zhou, J. Chen, S. Lu, Z. Tang, Z. Shi, H. Zhu, Y. Zhang, F. Liu, *Adv. Sci.* **2022**, *9*, 2104613.

[56] S. Ullbrich, J. Benduhn, X. Jia, V. C. Nikolis, K. Tvingstedt, F. Piersimoni, S. Roland, Y. Liu, J. Wu, A. Fischer, D. Neher, S. Reineke, D. Spoltore, K. Vandewal, *Nat. Mater.* **2019**, *18*, 459-464.

[57] Y. Tamai, Y. Murata, S.-i. Natsuda, Y. Sakamoto, *Adv. Energy Mater.* **2024**, *14*, 2301890.

[58] H. Jin, N. Mallo, G. Zhang, O. Lindsay, R. Chu, M. Gao, S. McAnally, I. M. Etchells, P. L. Burn, I. R. Gentle, P. E. Shaw, *Adv. Funct. Mater.* **2024**.

[59] T. A. Dela Peña, R. Ma, Z. Xing, Q. Wei, J. I. Khan, R. M. Young, Y. Hai, S. A. Garcia, X. Zou, Z. Jin, F. L. Ng, K. L. Yeung, D. F. Swearer, M. R. Wasielewski, J. Wang, H. Cha, H. Yan, K. S. Wong, G. Li, M. Li, J. Wu, *Energy Environ. Sci.* **2023**, *16*, 3416-3429.

[60] A. A. Sifat, J. Jahng, E. O. Potma, *Chem. Soc. Rev.* **2022**, *51*, 4208-4222.

[61] X. Wei, L. Jia, B. Duan, X. Wang, L. Du, S. Li, Z. Xu, W. Zhao, *Adv. Funct. Mater.* **2024**, *34*, 2408960.

[62] Z. Wang, K. Gao, Y. Kan, M. Zhang, C. Qiu, L. Zhu, Z. Zhao, X. Peng, W. Feng, Z. Qian, X. Gu, A. K. Y. Jen, B. Z. Tang, Y. Cao, Y. Zhang, F. Liu, *Nat. Commun.* **2021**, *12*, 332.

[63] R. Ma, X. Jiang, J. Fu, T. Zhu, C. Yan, K. Wu, P. Müller-Buschbaum, G. Li, *Energy Environ. Sci.* **2023**, *16*, 2316-2326.

[64] Y. Zou, Y.-S. Hu, D.-H. Tian, H. Wu, X. Lv, G. Jiang, Y.-X. Huang, *Chinese Chem. Lett.* **2024**, *35*, 109090.

[65] H. Bai, Q. Fan, R. Ma, X. Guo, W. Ma, M. Zhang, *Chinese J. Chem.* **2024**, *42*, 1307-1318.

[66] Z. Li, X. Kong, Y. Liu, H. Qiu, L. Zhan, S. Yin, *Chinese Chem. Lett.* **2024**, *35*, 109378.

[67] R. Ma, H. Li, T. A. Dela Peña, H. Wang, C. Yan, P. Cheng, J. Wu, G. Li, *Natl. Sci. Rev.* **2024**, *11*, nwae384.